 CMES, vol.118, no.1, pp.177-205, 2019

Effects of the Convex Topography on Railway Environmental Vibrations

Huaxi Lu[1, *], Zhicheng Gao[1], Luyao Xu[1] and Bitao Wu[1]

Abstract: The railway environmental vibration caused by high-speed railways is harmful to the human health, the structural safety of adjacent buildings, and the normal use of precision instruments. At the same time, it occurs frequently. In this case, the railway environmental vibration has drawn much attention with the rapid development of high-speed railways. Studies in Earthquake Engineering show that a convex topography has a great impact on ground vibrations, however, there is no consideration about the convex topographic effect in the study of the railway environmental vibration when the convex topography is near the roadway. In this paper, the influence of a convex topography on the railway environmental vibration was investigated. Two-dimensional (2D) finite element models consist of subgrade-convex topography and subgrade-flat topography are established using the finite element method. The length and the height of the analysis model are taken as 200 m and 41.3 m, respectively. The external soil of the calculation model is simulated via the artificial boundary. By comparison with measured results, the 2D finite element models were verified to be effective. The convex topographic effect is studied by conducting parameter investigations, such as the bottom width, cross-sectional shape, height-width ratio and the foundation soil properties. Results show that the dimension and cross-section shape of the convex topography and the foundation soil properties have significant effect on the convex topographic effect.

Keywords: Railway environmental vibration, convex topography, ground acceleration, ground displacement, frequency spectra.

1 Introduction

The railway environmental vibration has a serious impact on the human health, the structural safety of adjacent buildings, and the normal use of precision instruments. In this context, the railway environmental vibration has become a topic of great concern to international academic circles, scholars have done a lot of research on it [Xia, Cao and Roeck (2010); Zhang and Feng (2011); Hesami, Ahmadi and Ghalesari (2016)].

Some scholars have conducted experiments on the railway environmental vibration and obtained a large amount of important data. Krylov [Krylov (1997)] conducted a field test on ground vibration response between Courtalain and Tours in France to verify the critical speed phenomenon. In the test, high levels of ground vibrations were observed

[1] Department of Civil Engineering, East China Jiaotong University, Nanchang, 330013, China.

[*] Corresponding Author: Huaxi Lu. Email: 2512@ecjtu.jx.cn.

when the TGV high-speed train passed. Kim et al. [Kim and Lee (2000)] found that the frequency range of the railway environmental vibration was 7-70 Hz by field tests, and the train speed had little effect on the main frequency range. Degrande et al. [Degrande and Schillemans (2001)] measured the free field vibrations and track response during the passage of a high-speed train between Brussels and Paris. Their experimental results provided a lot of measured data for the validation of numerical prediction model and were widely referenced.

Takemiya [Takemiya (2008)] conducted field measurements for the passage of the Shinkansen high speed trains on viaducts and found that vibrations were dominated by low frequency under deep soft soil conditions and by high frequency under shallow soft soil conditions. Chen et al. [Chen, Zhao, Wang et al. (2013)] constructed a full-scale model of ballastless track-subgrade to find the dynamic load magnification factor for ballastless track-subgrade of high-speed railway. Connolly et al. [Connolly, Costa, Kouroussis et al. (2015)] analyzed over 1500 ground-borne vibration records, at 17 high speed rail sites, across 7 European countries. The study provides new insights into characteristics and uncertainties in railway ground-borne vibration prediction. The influence of topography is considered in these experiments and analyses.

Another part of scholars carried out theoretical analyses adopting numerical analysis method. Taniguchi et al. [Taniguchi and Sawada (1979)] investigated the propagation characteristics of the traffic-induced vibrations and proposed a prediction method of the attenuation with distance of the traffic-induced vibrations. They found that the Rayleigh wave is dominant in the traffic-induced vibrations. The studies of the numerical simulation completed by Auersch et al. [Auersch and Reitan (1994); Auersch (2008); Auersch (2012)] showed that the stiffness, damping and layer thickness of the ground soil had a great influence on the amplitudes and frequency spectra of railway vibrations. Jones et al. [Jones, Houedec and Peplow (1998a); Jones, Houedec and Petyt 1998(b)] studied the displacement responses of the ground surface subjected to a moving rectangular harmonic vertical load using a double Fourier transform.

Sheng et al. [Sheng, Jones and Petyt (1999)] established the prediction model of ground vibrations by the layering method and obtained the vibration response of the track structure and layered soil subjected to a moving load by numerical calculation. Connolly et al. [Connolly, Giannopoulos and Forde (2013)] presented a 3D numerical model which was capable of modelling the propagation and transmission of ground vibration in the vicinity of high speed railways and found that soft embankments would increase the vibration levels of the surrounding soil. Kouroussis et al. [Kouroussis, Conti and Verlinden (2013)] studied the influence of the dynamic and geometrical soil parameters on the propagation of ground vibrations induced by external loads. Lopes et al. [Lopes, Costa, Ferraz et al. (2014)] proposed a numerical approach for the prediction of vibrations included in buildings due to railway traffic in tunnel. Using the proposed model, they study the impact of the use of floating slabs systems for the isolation of vibrations in the tunnel on the response of a building located in the surrounding of the tunnel.

A review of the above literatures reveals that most of current studies on the railway environmental vibration are based on flat topography. However, the convex topography is actually widespread along the railway. Studies on the convex topography in the

earthquake engineering found the horizontal vibration is amplified by the convex topography when the seismic wave is incident on a convex topography, and the vertical vibration is also amplified under certain conditions [Liu (1996); Sohrabi-Bidar, Kamalian and Jafari (2010); Sohrabi-Bidar and Kamalian (2013)]. This finding can be expanded to the railway environmental vibration, but the railway environmental vibration and earthquake are different in the durations, spectrum characteristic and intensities. Therefore, it is of theoretical and practical significance to study the vibration response characteristics of the convex topography under high-speed train loads.

In this paper, two calculation models of the subgrade-convex topography and the subgrade-flat topography subjected to high-speed train loads are established by finite software ANSYS. In present work, the vibration areas of interest are on the convex topography and the flat ground behind it. The way to establish 2D finite element models is showed in Section 2. In Section 3, the efficiency of present models is validated with measured results of a field test. The influence regularities of the width, cross-sectional shape and height-width ratio of the convex topography and the foundation soil properties on the railway environmental vibration are obtained by comparing the results of the two models in Section 4. Finally, some conclusions are given in Section 5.

2 Establishment of 2D finite element models

In the field of engineering and technology, for many mechanical and physical problems, the exact solution can be obtained analytically only in a few cases where the properties of the equation are simple and the geometry is quite regular. For most problems, we can use numerical methods to solve them. Because of versatility and effectiveness, the finite element method, a numerical method, has been widely used in engineering analysis [Hall (2003); Feng, Zhang, Zheng et al. (2017)]. Therefore, this paper uses the 2D finite element method to carry out some qualitative analysis.

2.1 Size of the models and cell grid

In the study of the vibration of railway subgrade, the influence of the boundary can be eliminated when the distance between the boundary and the track is greater than 30 m [Zhai (2007)]. Considering the calculation model contains the convex topography, the length and the height of the foundation are taken as 200 m and 41.3 m, respectively. In addition, the calculation accuracy of the finite element model can be improved by refining grids. Relatively accurate results can be obtained when the element length is 1/6 of the minimum shear wavelength [Kuhlemeyer and Lysmer (1973); Kausel, Roesset and Christian (1976)]. According to the frequency of the train-induced vibration and the condition of the foundation, the length of the element mesh of the calculation models is 0.5 m.

2.2 Integral time step

A reasonable integration time step can produce more accurate results in the transient analyses of the models. On one hand, if the time step is too large, the calculation result will lose part of the high-frequency component, and the calculation accuracy will decrease or the calculation results will be divergent. On the other hand, if the time step size is too small, the efficiency of the calculation will be affected. For elastic wave

effects, the integral time step should satisfy the following equation:

$$\Delta t \le L / C_0 \tag{1}$$

in which L is the length of the finite element mesh, and C_0 is the wave velocity. Therefore, the integral time step is 5 ms in this paper, and it was found that the reasonable accuracy could be produced by this time step in the trial.

2.3 Damping

When the train-induced vibrations propagate in the soil, the energy of the vibrations will decrease with the increase of the distance from the source of vibration, because of damping. The Rayleigh damping is generally used in dynamic analysis, and it can be written as follows:

$$[C] = \alpha [M] + \beta [K] \tag{2}$$

where α is the viscous damping component, β is the damping component of the solid stiffness, M is the mass matrix, and K is the stiffness matrix. The railway environmental vibration studied in this paper is related to the micro vibration, so the α and β can be determined by

$$\alpha = \frac{2\omega_j \omega_k}{\left(\omega_j + \omega_k\right)} \xi \ , \ \beta = \frac{2\xi}{\omega_j + \omega_k} \tag{3}$$

In which ξ is the constant damping ratio, and the ω_j and ω_k are natural angular frequencies. The damping ratio of this paper is 0.03 [Ghayamghamian and Kawakami (2000)]. The predominant frequencies of the train-induced environmental vibration are around 7.5 Hz and 16 Hz, therefore the ω_i and ω_j are separately taken as $7.5\times2\pi$ rad/s and $16\times2\pi$ rad/s. Thus the α and β are 3.35 and 0.00071, respectively.

2.4 Artificial boundary

The artificial boundary is employed to simulate external soil of the calculation model in the study of the railway environmental vibration. The viscous-spring artificial boundary [Liu and Lu (1998)] is selected and modeled by element COMBIN14. The viscous-spring artificial boundary which belongs to the local artificial boundary has the characteristic of spatiotemporal decoupling and can reduce the calculating time. At the same time, the viscous-spring artificial boundary, which has an elastic recovery performance, can better simulate the half-space system and make the frequency more stable. Each viscous boundary element contains two spring and damping elements. The spring constant (K_B) and damping coefficient (C_B) of the 2D viscous-spring artificial boundary equivalent physical system are as follows:

Tangential boundary

$$K_{BT} = \alpha_T \frac{G}{R}, C_{BT} = \rho c_S \tag{4}$$

Normal boundary

$$K_{BN} = \alpha_N \frac{G}{R}, C_{BN} = \rho c_P \tag{5}$$

where K_{BT} and K_{BN} are the tangential and normal stiffness of the spring, respectively; R is the distance between wave source and artificial boundary; c_S and c_P are the wave velocities of the s-wave and p-wave, respectively; G and ρ are the shear modulus and density of the medium, respectively; α_T and α_N are the tangential and normal viscous-spring artificial boundary parameters, respectively. The ranges of α_T and α_N are 0.35~0.65 and 0.8~1.2, respectively. α_T and α_N are taken as 0.5 and 1.0, respectively.

2.5 Train load simulation

The train load [Jenkins, Stephenson, Clayton et al. (2000)] can be simulated by

$$F(t) = k_1 k_2 (P_0 + P_1 \sin \omega_1 t + P_2 \sin \omega_2 t + P_3 \sin \omega_3 t) \tag{6}$$

where k_1 is the superposition coefficient, k_2 is the dispersion coefficient and P_0 is the unilateral static wheel load; P_1, P_2 and P_3 are the typical amplitudes of control conditions of the low frequency, medium frequency and high frequency, respectively. k_1 and k_2 are generally 1.2~1.7 and 0.6~0.9 respectively. In this paper, k_1 and k_2 are 1.6 and 0.7 respectively. P_1, P_2 and P_3 are expressed as follows:

$$P_i = M_0 \alpha_i \omega_i^2 \tag{7}$$

where M_0 denotes the unsprung mass of train; α_i are the typical vector heights of low frequency, medium frequency and high frequency; ω_i are the circular frequencies of unsmoothed vibration wavelengths of the low frequency, medium frequency and high frequency at a certain train speed. ω_i is given by

$$\omega_i = 2\pi \frac{v}{L_i} \tag{8}$$

where v denotes the train speed; L_i are typical unsmoothed vibration wavelengths of the low frequency, medium frequency and high frequency. The relevant parameters of CHR1 are as follows: The axle load is 16 t, the unilateral static wheel load P_0 is 80 kN, and the unsprung mass M_0 of the train is 750 kg. The typical unsmoothed vibration wavelengths and vector heights of the low frequency, medium frequency and high frequency are L_1=10 m and α_1=3.5 mm, L_2=2 m and α_2=0.4 mm, and L_3=0.5 m and α_3=0.08 mm, respectively.

For the 2D model, the vertical load on the subgrade is evenly distributed along the line in the length range of the train, so the train load $F(t)$ can be equivalent to the load $F_1(t)$, which distributes uniformly along the line. $F_1(t)$ is given by

$$F_1(t) = K_C \cdot n \cdot N \cdot F(t) / L_T \tag{9}$$

where K_C is the correction coefficient, n is the number of the wheel set in each carriage, N is the number of carriages and L_T is the train length. As a result of the dispersal effect of the rails and sleepers on the loads transferred from the train to the surface of ballast bed, the empirical value of K_C is generally 0.6~0.9. K_C is taken as 1, since the unballasted track was used in this paper.

In the verification analysis the train speed is 350 km/h as same as the reference, and the train speed is taken as 250 km/h throughout Section 4. The simulated time-history curve of the load $F_1(t)$ at the speed of 250 km/h is shown in Fig. 1.

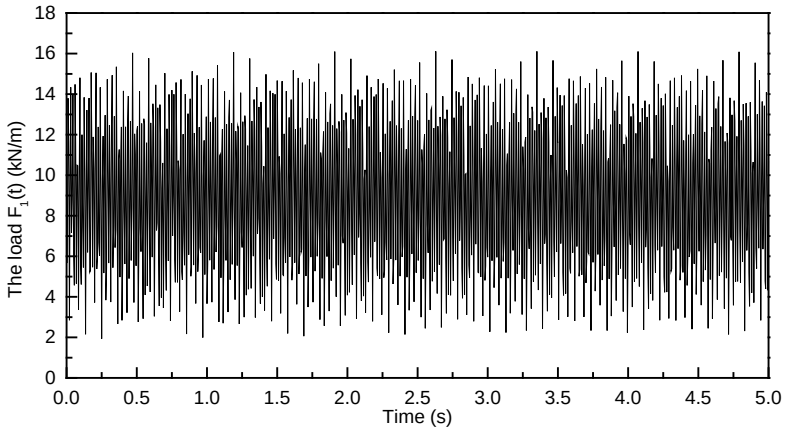

Figure 1: Load $F_1(t)$ at the speed of 250 km/h

2.6 Subgrade and calculation models

The high-speed railway subgrade is adopted in the model. According to the design specification for high-speed railways in China, the subgrade consists of three layers of soil. The specific parameters of each layer of soil in the subgrade are as shown in Tab. 1 [Shao, Wei and Han (2013)]. The above subgrade is adopted in the full text. Element PLANE42 is used to mesh the subgrade and foundation soil. Based on the above theories, the 2D finite element models were established as shown in Fig. 2. The distance between the center of the convex topography and track is 55 m.

Table 1: Parameters

	Thickness (m)	Elastic modulus (Mpa)	Poisson's ratio	Damping ratio	Shear wave velocity (m/s)	Density (kg/m^3)
First layer	0.4	150	0.25	0.038	174	1900
Second layer	2.3	110	0.25	0.034	145	1950
Third layer	3.6	50	0.35	0.03	100	1900

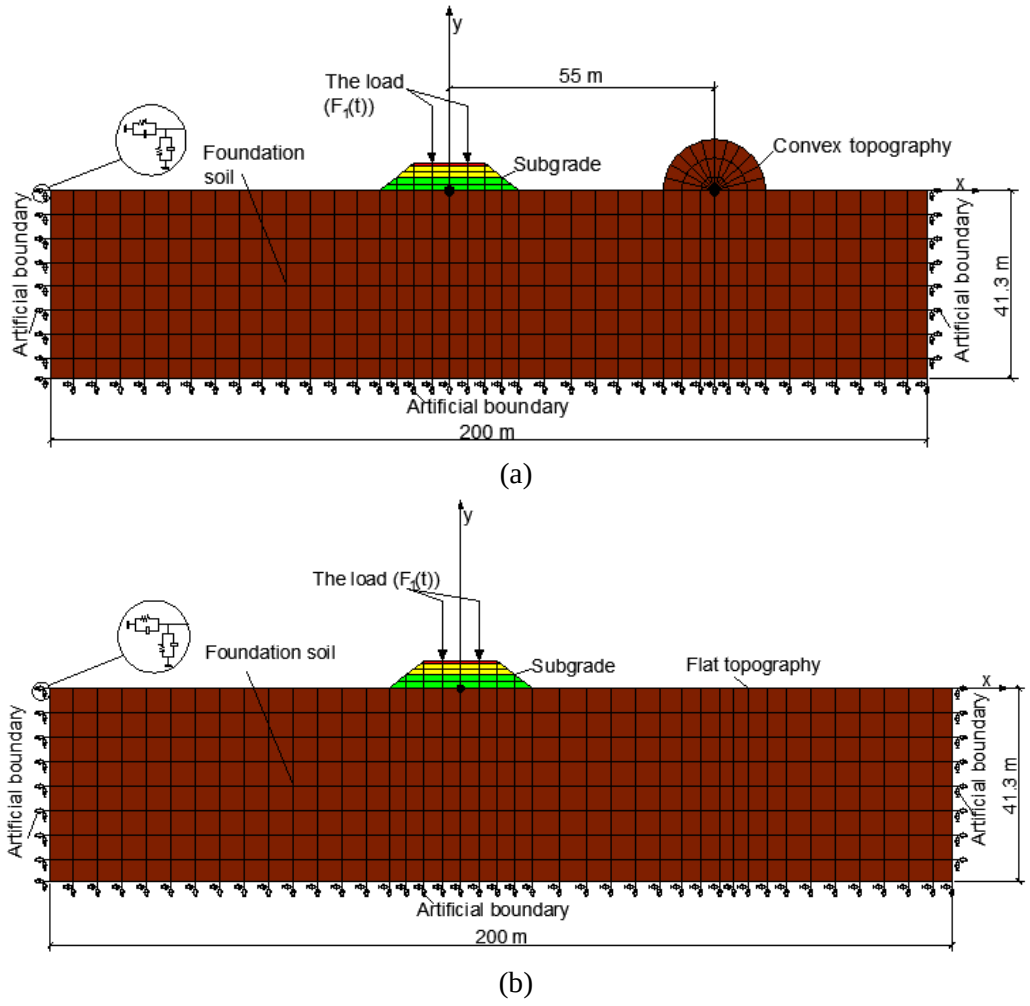

Figure 2: 2D finite element models. (a) subgrade-convex topography. (b) subgrade-flat topography

3 Validation of the present 2D finite element models

To verify the validity of the 2D finite element models, the measured results of a high-speed railway in a soft soil area is considered as a reference. The measured train speed is 350 km/h, and there are four layers of foundation soil in the reference, and the parameters of each layer of the foundation soil are shown in Tab. 2 [Shao, Wei and Han (2013)]. The established 2D finite element validation model is shown in Fig. 3. Fig. 4 shows the present simulation results and measured results of the peak vertical ground acceleration at different distances from the center of the track. The present simulation results are in good agreement with the measured results. That means the models established in this paper are reasonable in meshing, boundary conditions and loading. Hence, the models can be utilized to progress the problem of the railway environmental vibration effectively.

Table 2: Parameters layered soil of the validation model layered soil

	Thickness (m)	Elastic modulus (Mpa)	Poisson's ratio	Damping ratio	Shear wave velocity (m/s)	Density (kg/m^3)
First layer of soil	7.5	20	0.29	0.03	64	1898
Second layer of soil	10.5	40	0.3	0.02	88	2000
Third layer of soil	12.5	74	0.31	0.019	124	1847
Fourth layer of soil	4.5	141	0.33	0.01	167	1900

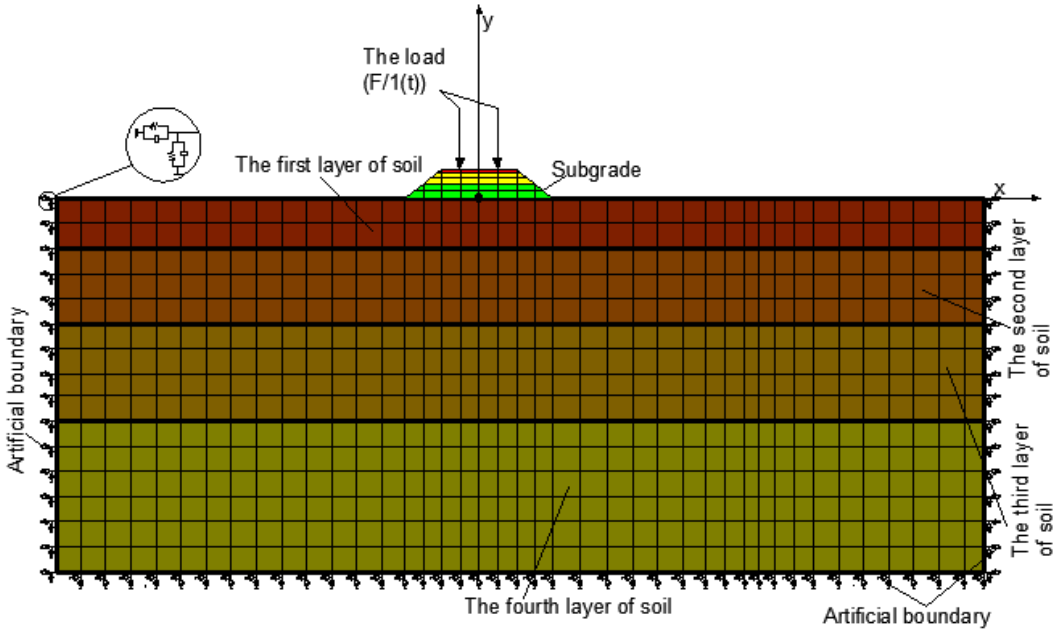

Figure 3: Calculation model for validation

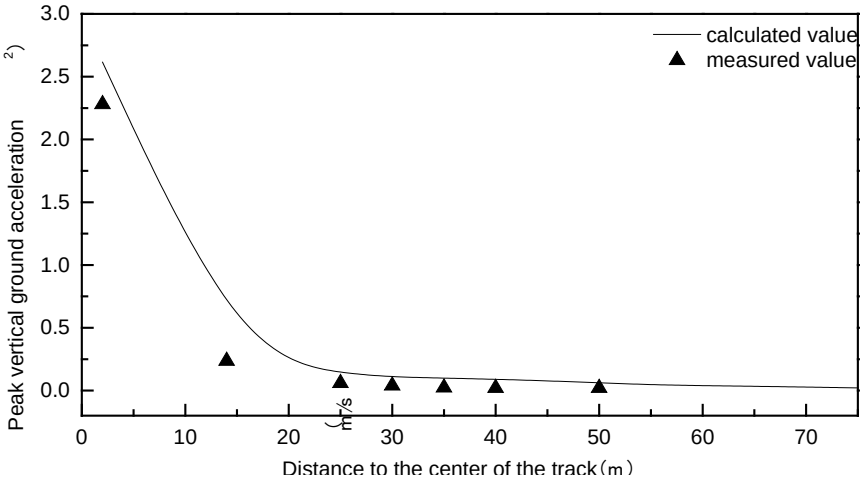

Figure 4: Peak vertical ground acceleration

4 Parameter analysis of the convex topography

The surface wave (R wave) and body wave (P wave and S wave) are generated in homogeneous sites under the moving train loads. The energy of the R wave is the largest, and its propagation distance is the farthest. When the train runs on the flat topography, the ground vibration is the result of the superposition of the R wave and the P wave and S wave propagating near the ground, as shown in Fig. 5(a). Fig. 5(b) shows the waves are diffracted at the foot of the convex topography, and the ground vibration is more complicated due to the convex topography.

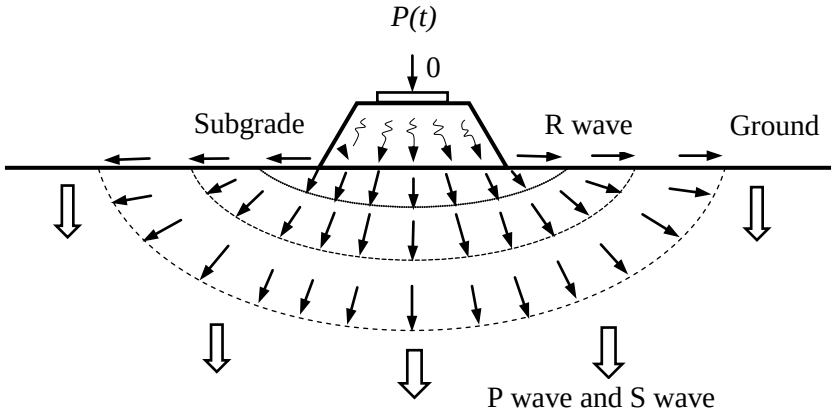

(a)

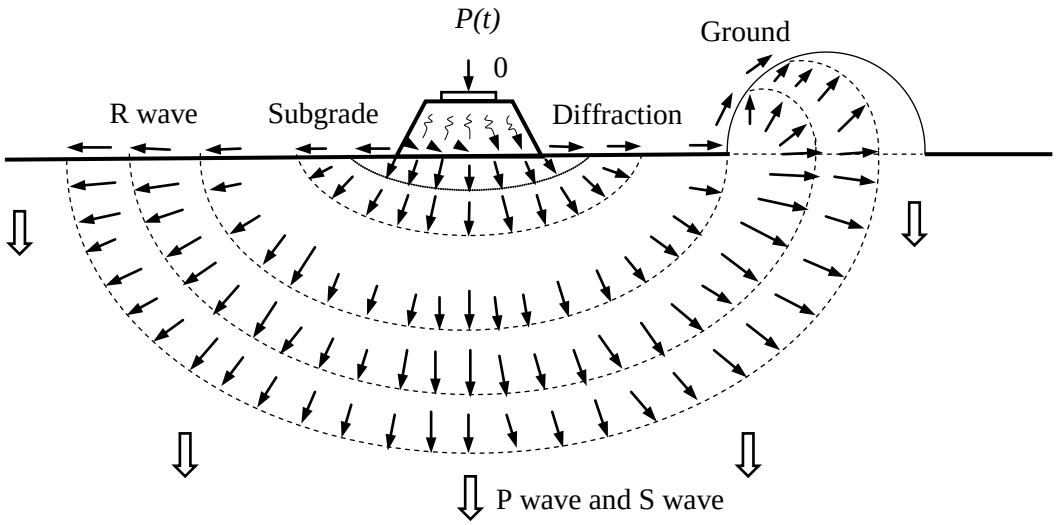

(b)

Figure 5: The schematic diagram of vibration propagation induced by trains. (a) The flat topography (without a convex topography). (b) The convex topography

Using the established 2D finite element models, the influence regularities of parameters of the convex topography on the train-induced vibration are investigated. As already stated in Section 1, the vibration areas of interest are on the convex topography and the flat ground behind it. The results of the study can be obtained via comparing the responses of the ground surface at the same coordinates in the X axis in the models. In order to simplify the analysis, for the flat ground behind the convex topography, the observation point for analyses is 90 m from the center of the track.

4.1 Influence of the bottom width of the convex topography

The convex semi-circular topographies with bottom widths (**D**) of 30 m, 50 m and 70 m are researched, respectively. The 2D finite element models are shown in Fig. 6 and Fig. 2(b). The homogeneous foundation, which has an elastic modulus of 74 Mpa, Poisson's ratio of 0.31, density of 1847 kg/m^3, and shear wave velocity of 124 m/s, has been used in this section. This homogeneous foundation is also used in the Subsections 4.2 and 4.3. The subgrade described in Subsection 2.6 is adopted throughout Chapter 4, and the specific parameters of the subgrade are shown in Tab. 1.

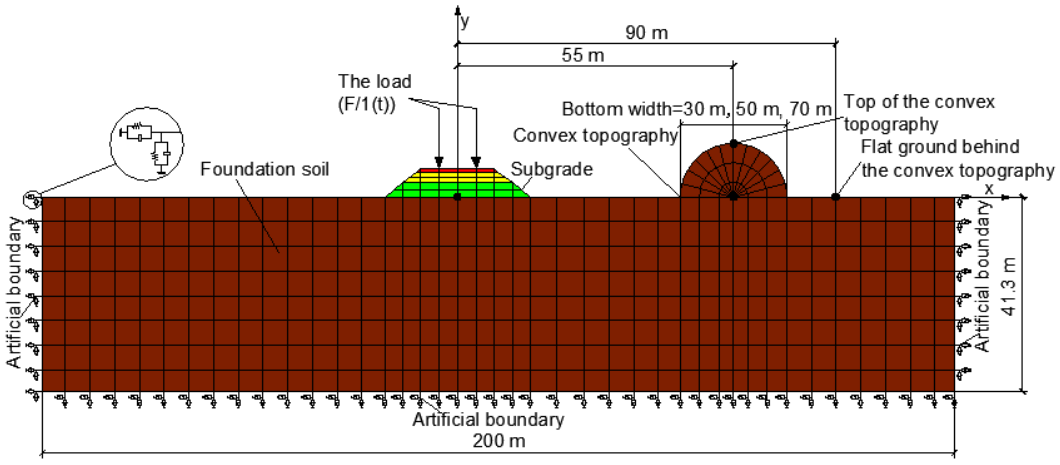

Figure 6: Calculation model of a subgrade-convex topography for convex topographies with various bottom widths

It can be seen from the Fig. 7 that the vertical ground acceleration (VGA) and the horizontal ground acceleration (HGA) on the convex topography decrease obviously due to the scattering by a convex topography, and the bottom width has little effect on the VGA and HGA. As shown in Fig. 8, comparing with the flat topography (without a convex topography), the vertical ground displacement (VGD) and the horizontal ground displacement (HGD) on the convex topography are both amplified, and the amplification effects are more obvious with the increase of the bottom width. The amplification effect of the HGD is more significant than that of the VGD. Namely, the HGD at the top of the convex topography with a bottom width of 30 m is amplified 2.05 times, and the VGD is only amplified 1.14 times. As the bottom width increased to 70 m, the HGD is amplified 3.03 times, and the VGD is only amplified 1.14 times.

For the flat ground behind the convex topography (90 m from the track centerline), Fig. 7 shows that the VGA and HGA are also significantly reduced by the convex topography. The decreased amplitudes of the VGA and HGA increase with the increase of the bottom width. Moreover, Fig. 8 shows the VGD is decreased due to the convex topography. However, the decreased amplitude of the VGD is decreased as the bottom width increases. On the contrary, the HGD are amplified, and the amplification effect is more obvious with the increase of the bottom width.

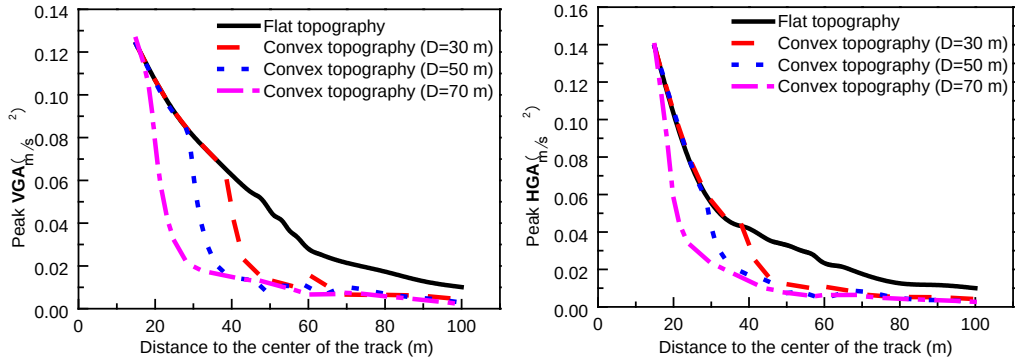

(a) (b)

Figure 7: Peak ground accelerations of the convex topographies with different bottom widths

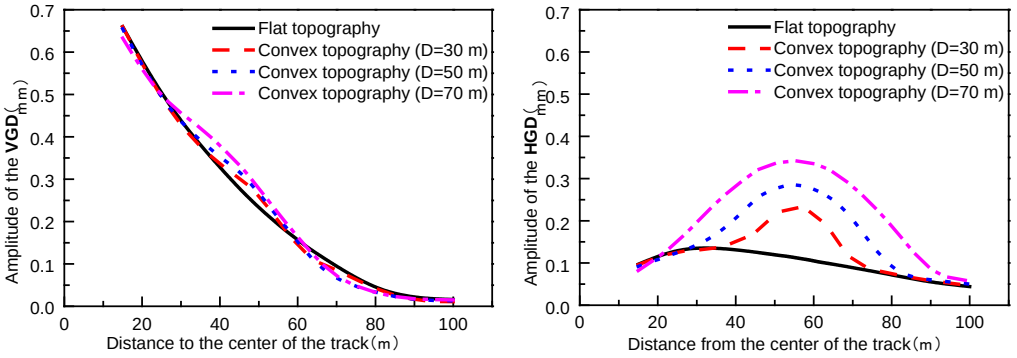

(a) (b)

Figure 8: Amplitudes of ground vibration displacements of the convex topographies with different bottom widths

Fig. 9 shows the frequency spectrum curves of the top of the convex topography and the flat ground behind it. Due to the impacts of the convex topography, the vertical and horizontal high-frequency components (20-25 Hz) of the top of the convex topography and the flat ground behind it are obviously attenuated. Furthermore, the vertical and horizontal high-frequency components (20-25 Hz) on the flat ground behind the convex topography are more obviously attenuated with the increase of the bottom width of the convex topography.

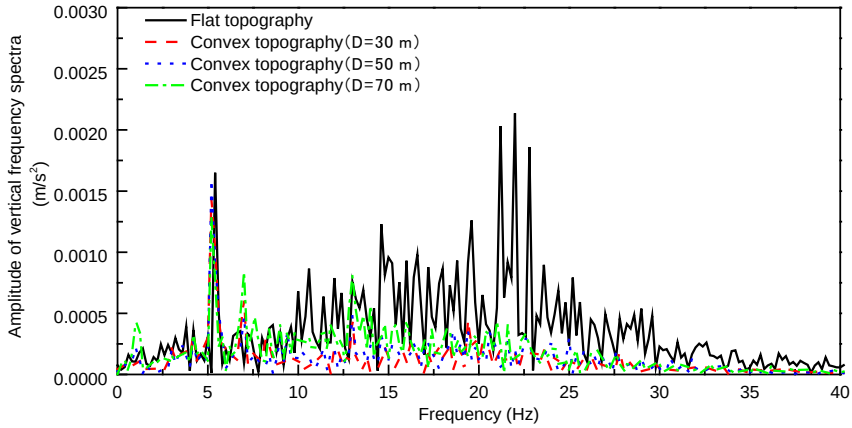
Flat topography
Convex topography（D=30 m）
Convex topography（D=50 m）
Convex topography（D=70 m）
Amplitude of vertical frequency spectra (m/s²)
Frequency (Hz)
0.0030
0.0025
0.0020
0.0015
0.0010
0.0005
0.0000
0
5
10
15
20
25
30
35
40

(a)

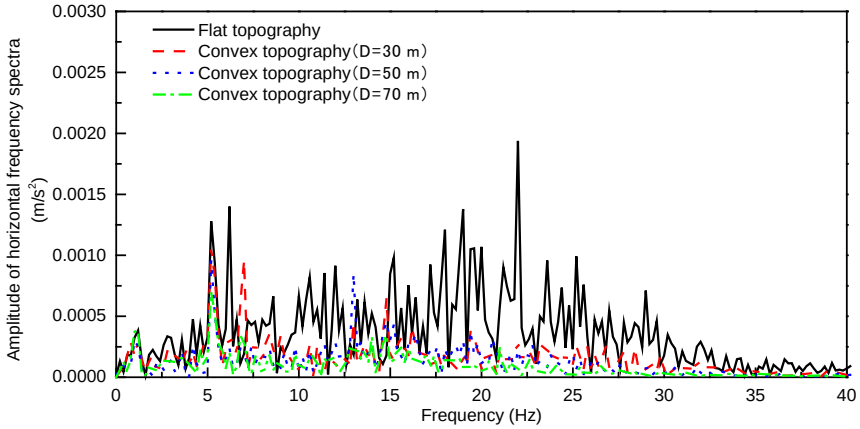
Flat topography
Convex topography（D=30 m）
Convex topography（D=50 m）
Convex topography（D=70 m）
Amplitude of horizontal frequency spectra (m/s²)
Frequency (Hz)
0.0030
0.0025
0.0020
0.0015
0.0010
0.0005
0.0000
0
5
10
15
20
25
30
35
40

(b)

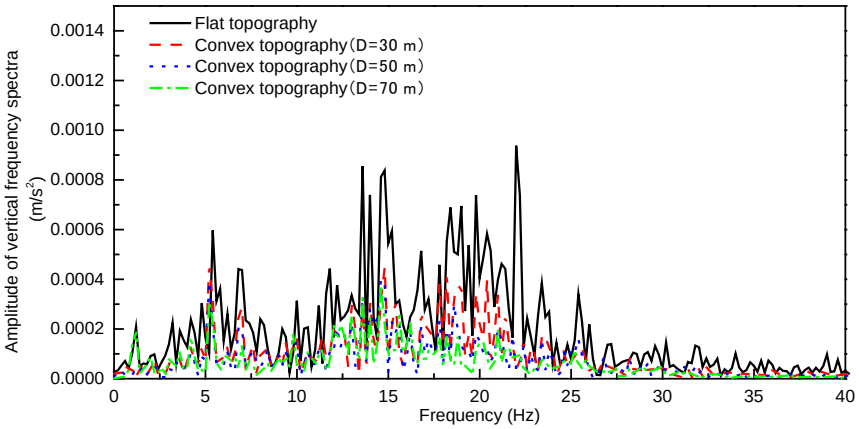
Flat topography
Convex topography（D=30 m）
Convex topography（D=50 m）
Convex topography（D=70 m）
Amplitude of vertical frequency spectra (m/s²)
Frequency (Hz)
0.0014
0.0012
0.0010
0.0008
0.0006
0.0004
0.0002
0.0000
0
5
10
15
20
25
30
35
40

(c)

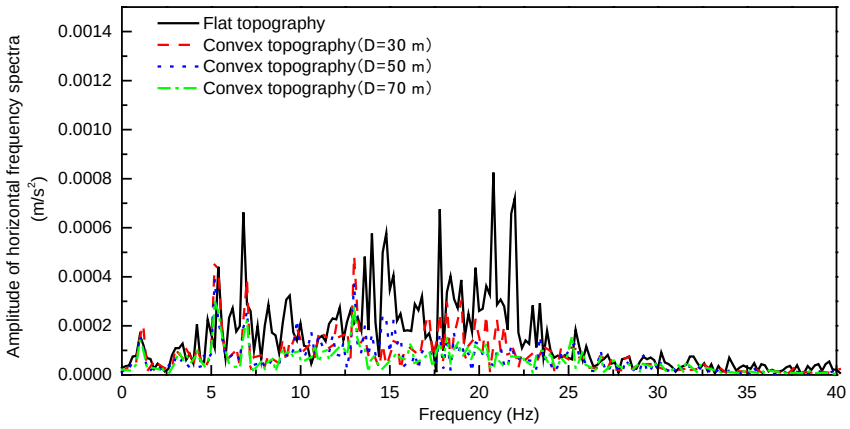

(d)

Figure 9: Frequency spectra for different bottom widths of the convex topographies. (a) Vertical frequency spectra of the top of convex topographies. (b) Horizontal frequency spectra of the top of convex topographies. (c) Vertical frequency spectra of the flat ground behind the convex topographies. (d) Horizontal frequency spectra of the flat ground behind the convex topographies

4.2 Influence of the cross-sectional shape of the convex topography

The triangle, trapezoid, and semicircle are selected as the cross sections to study the influence of the cross-sectional shape of the convex topography. The 2D finite element calculation model is shown in Fig. 10 and Fig. 2(b). The width and height of the convex topographies are 30 m and 15 m, respectively.

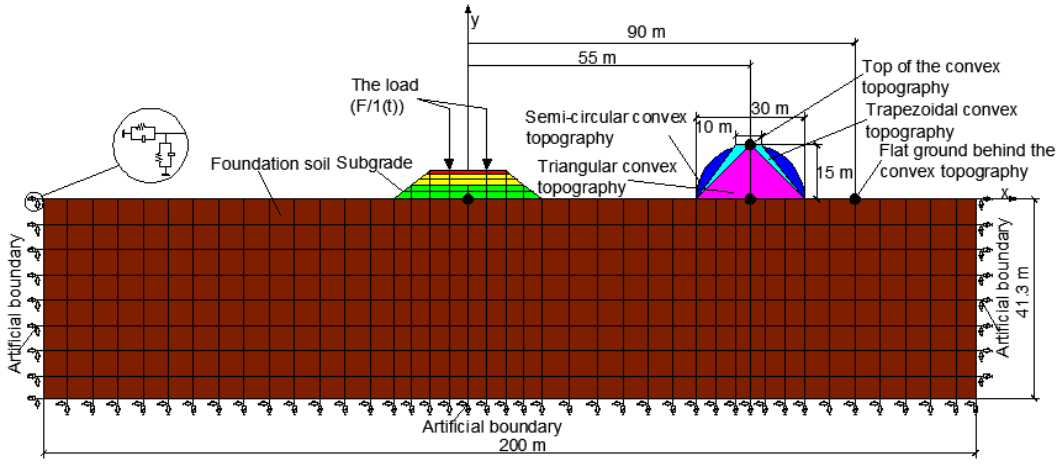

Figure 10: Calculation models of the subgrade-convex topography for the convex topographies with three kinds of cross-sectional shapes

Fig. 11 and Fig. 12 show that the impacts of the trapezoidal and semi-circular convex topographies on the VGA, HGA, VGD and HGD are close to the same on the convex topography (40 m to 70 m from the track centerline). The impacts of the triangular convex topography on the VGA and VGD are equivalent to those of the trapezoidal and semi-circular convex topography, but there are distinct differences on the HGA and HGD. For instance, the HGD of the triangular convex topography is amplified more obviously than those of trapezoidal and semi-circular convex topographies. In detail, the HGD at the top of the triangular convex topography is amplified 2.30 times by comparing with the flat topography (without a convex topography), and the HGDs at the top of the trapezoidal and semicircular convex topographies are amplified 2.07 times and 2.05 times, respectively. The above results are caused by the energy concentration at the sharp top of the triangular convex topography.

Fig. 11 and Fig. 12 illustrate that the impacts of the convex topographies of three kinds of cross-sectional shapes on the ground vibration are similar on the flat ground behind the convex topography. Hence, the cross-sectional shape of the convex topography has little effect on the vibration of the flat ground behind the convex topography.

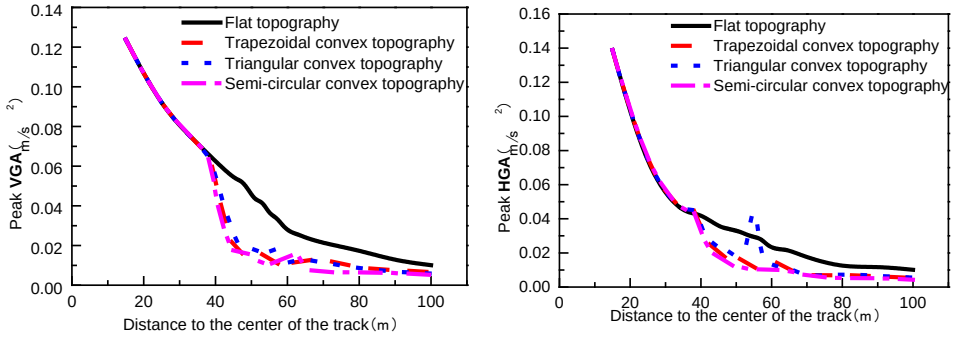

Figure 11: Peak accelerations of the convex topographies with three kinds of cross-sectional shapes

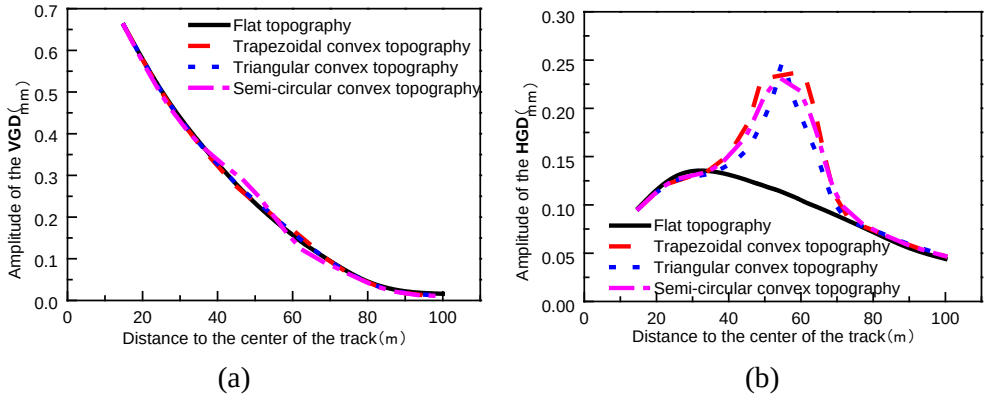

Figure 12: Amplitudes of ground vibration displacements of the convex topographies with three kinds of cross-sectional shapes

Fig. 13(a) and Fig. 13(b) show that for the top of the convex topography, the convex topographies of three kinds of cross-sectional shapes have similar effects on frequency spectrum characteristics, except that the triangular convex topography has an obvious local amplification effect in the horizontal direction. Fig. 13(c)) and Fig. 13(d) indicate that the convex topographies of three kinds of cross-sectional shapes also have consistent effects on the frequency spectrum characteristics of the flat ground behind the convex topography.

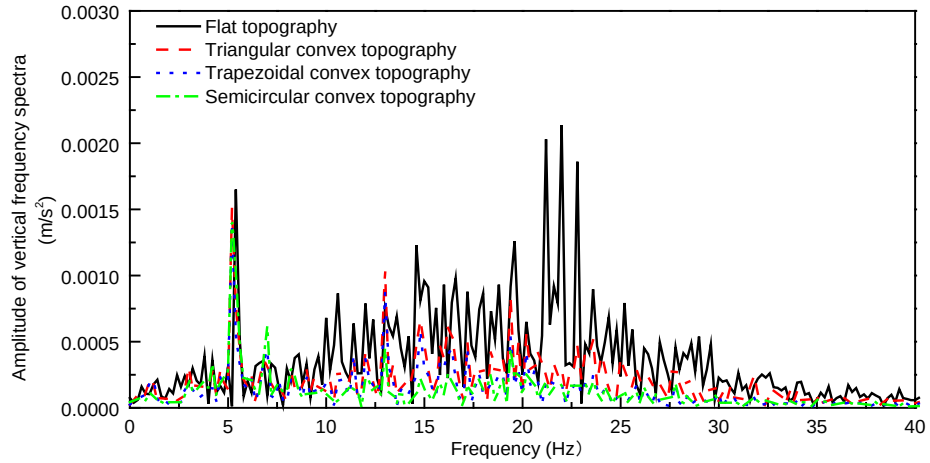

(a)

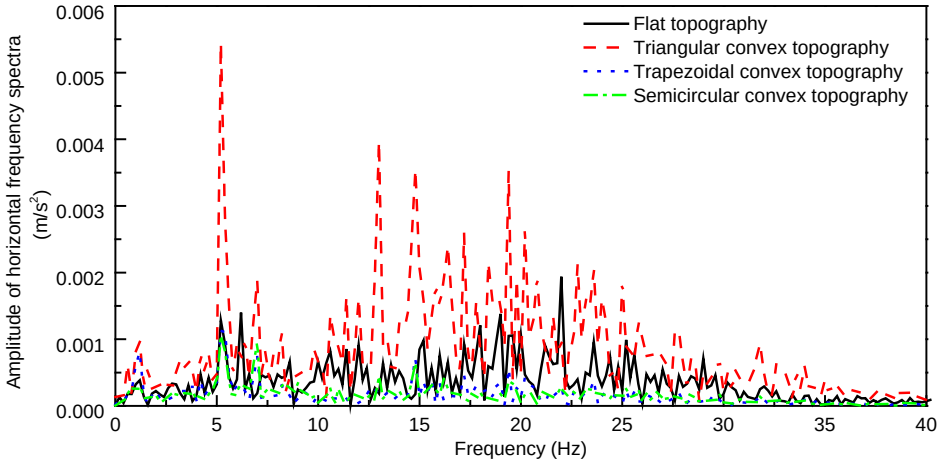

(b)

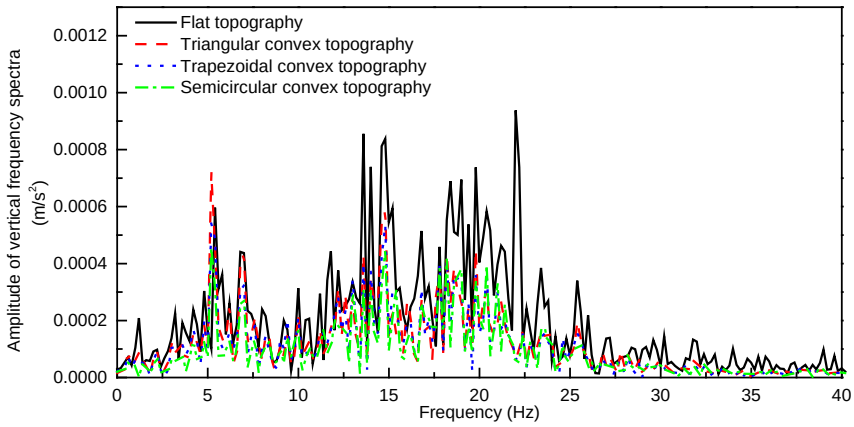

(c)

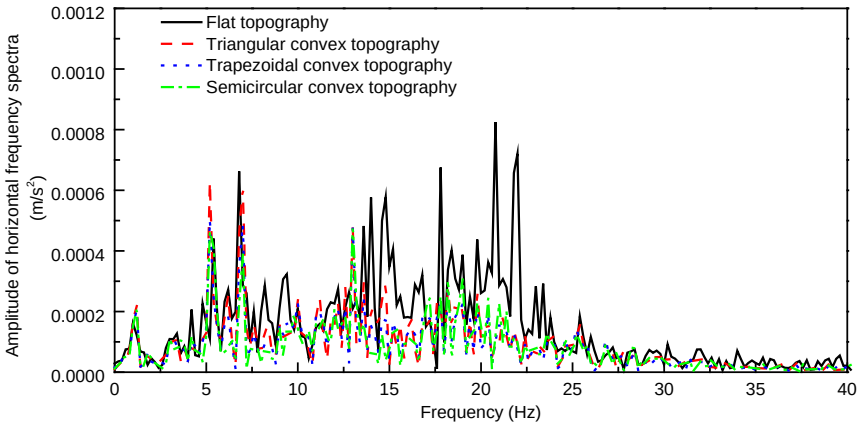

(d)

Figure 13: Frequency spectra for the convex topographies with different cross-sectional shapes. (a) Vertical frequency spectra of the top of convex topographies. (b) Horizontal frequency spectra of the top of convex topographies. (c) Vertical frequency spectra of the flat ground behind the convex topographies. (d) Horizontal frequency spectra of the flat ground behind the convex topographies

4.3 Influence of the height-width ratio of the convex topography

The height-width ratio (HWR) of the convex topography is the ratio of the height to the bottom width of the convex topography. The triangular convex topography with HWRs of 2.0, 1.0 and 0.5 are studied. Other calculation parameters of the 2D finite element calculation models are the same as the Subsection 4.2. The 2D finite element calculation models are shown in Fig. 14 and Fig. 2(b).

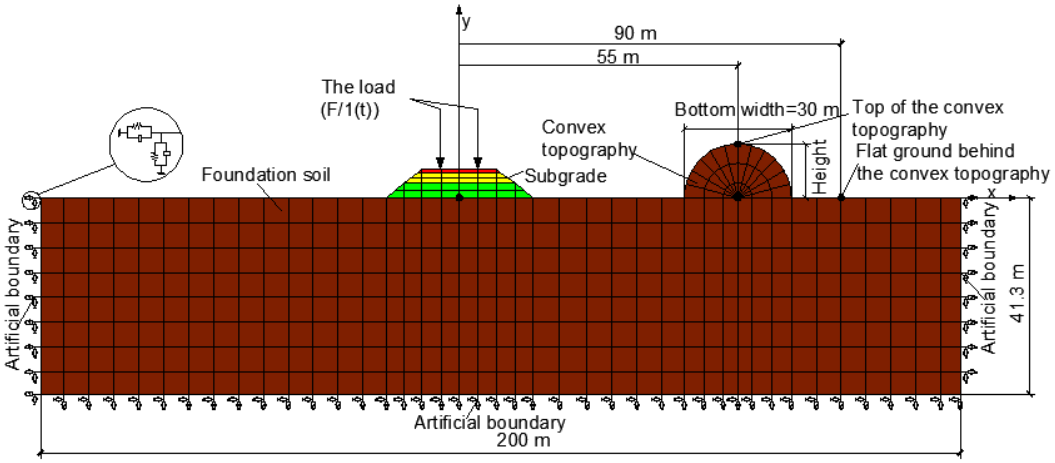

Figure 14: Calculation model of a subgrade-convex topography for the convex topographies with different height-width ratios

Fig. 15 and Fig. 16 demonstrate that the HWR has impacts on vibrations on the convex topography (40 m to 70 m from the track centerline). As shown in Fig. 15, the VGA and HGA on the convex topography decrease more obviously as the HWR increases. In addition, there is a local amplification effect at the top of the convex topography, and the increase of the HWR improves the local amplification effect of the convex topography on HGA. This could be that the bigger HWR makes the top of the triangular convex topography more sharp, and then the energy concentration is more obvious. Fig. 16 shows that although the HWR has a negligible effect on the VGD at the top of the convex topography, it has a significant impact on the HGD. As the HWR increases, the amplification effect of the convex topography on the HGD is more evident. We can see this phenomenon more clearly from the numerical value. Comparing with the flat topography (without a convex topography), the HGD at the top of the convex topographies with HWRs of 0.5, 1.0 and 3.0 are amplified 1.52, 2.30 and 3.10 times, respectively.

Fig. 15 and Fig. 16 show that the HWR has a little influence on the ground vibrations on the flat ground behind the convex topography. With the HWR increased, the ground vibrations on the flat ground behind the convex topography are almost unchanged.

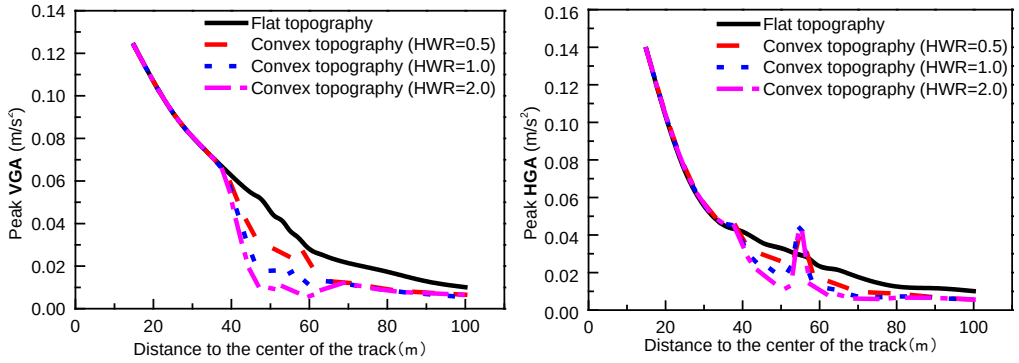

Figure 15: Peak accelerations of the convex topographies with different **HWR**s

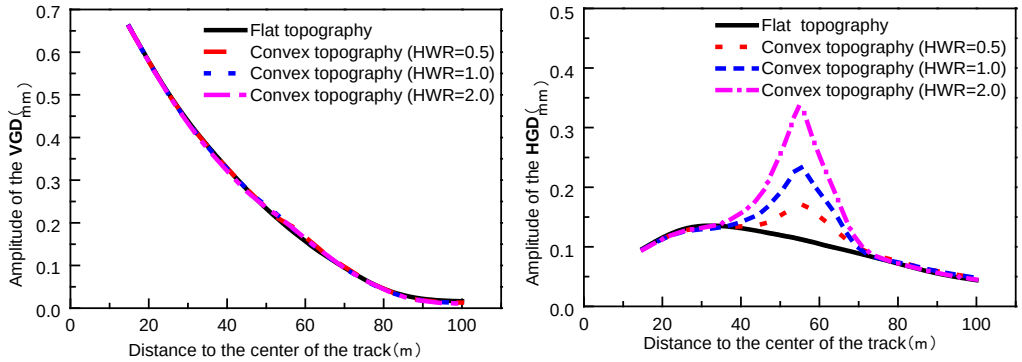

Figure 16: Amplitudes of ground vibration displacements of the convex topographies with different HWRs

As can be seen from Fig. 17(a) and Fig. 17(b), the increase of HWR results in more attenuation of the high-frequency components (20-25 Hz) of the vertical vibrations at the top of the convex topography. However, the low frequency components and high-frequency components of the horizontal vibrations are more obviously amplified with the increase of the HWR. Fig. 17(c) and Fig. 17(d) show that the increase of the HWR contribute to more attenuation of the vertical and horizontal high-frequency components (20-25 Hz) on the flat ground behind the convex topography.

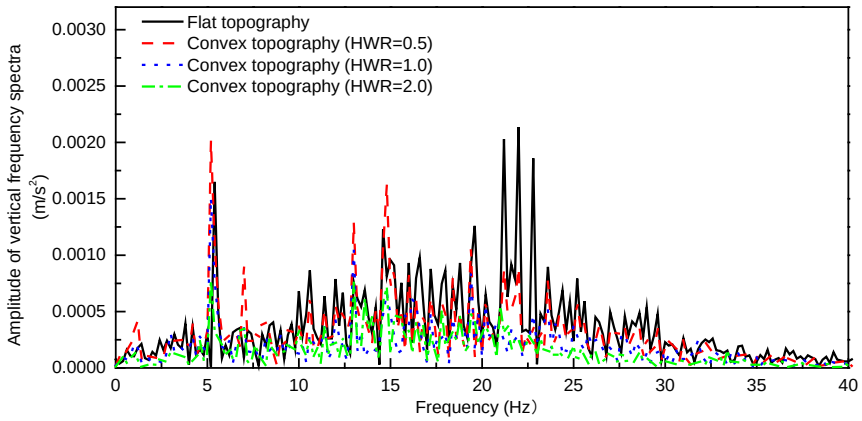
Flat topography
Convex topography (HWR=0.5)
Convex topography (HWR=1.0)
Convex topography (HWR=2.0)
Amplitude of vertical frequency spectra (m/s²)
Frequency (Hz)

(a)

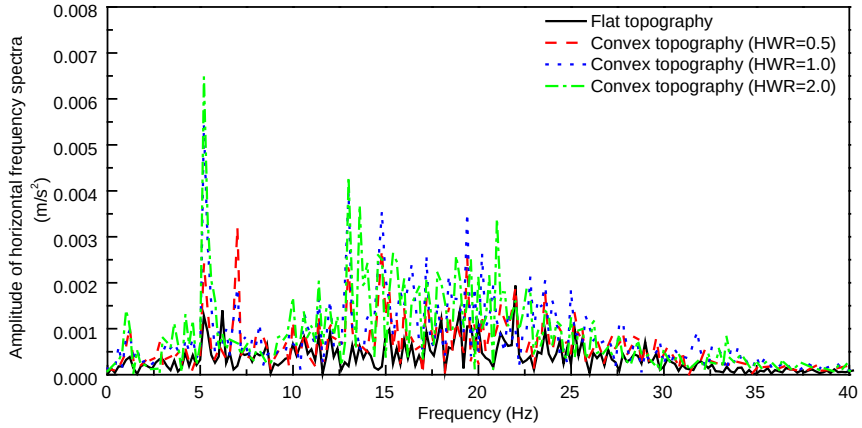
Flat topography
Convex topography (HWR=0.5)
Convex topography (HWR=1.0)
Convex topography (HWR=2.0)
Amplitude of horizontal frequency spectra (m/s²)
Frequency (Hz)

(b)

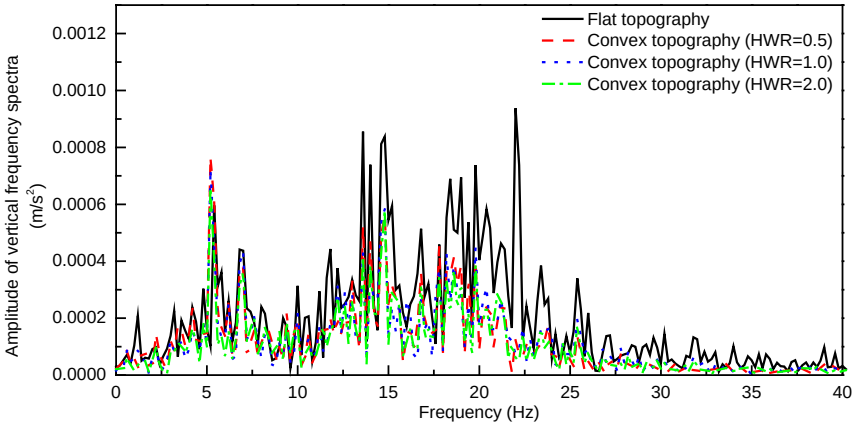
Flat topography
Convex topography (HWR=0.5)
Convex topography (HWR=1.0)
Convex topography (HWR=2.0)
Amplitude of vertical frequency spectra (m/s²)
Frequency (Hz)

(c)

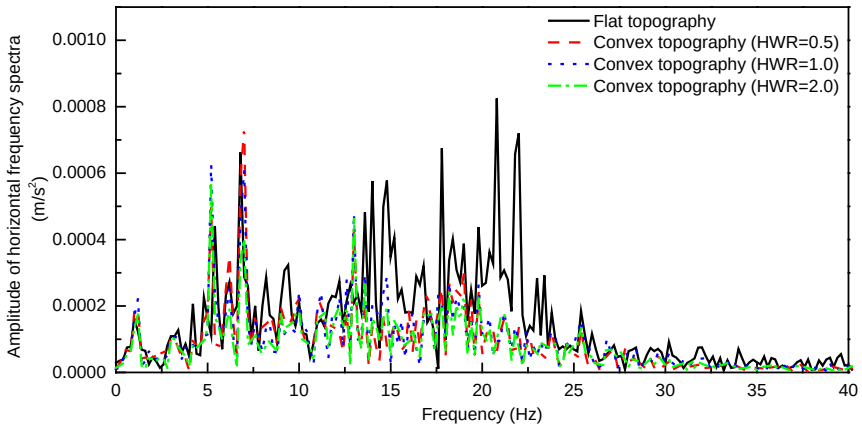

(d)

Figure 17: Frequency spectra for the convex topographies with different **HWR**s. (a) Vertical frequency spectra of the top of convex topographies. (b) Horizontal frequency spectra of the top of convex topographies. (c) Vertical frequency spectra of the flat ground behind the convex topographies. (d) Horizontal frequency spectra of the flat ground behind the convex topographies

4.4 Influence of the foundation soil properties

Three kinds of homogeneous foundations are compared and analyzed in this section. The bottom width and the height of the convex topography are 30 m and 15 m, respectively. The cross-sectional shape of the convex topography is a semicircle. The soil parameters of the homogeneous foundations are shown in Tab. 3. The established 2D finite element calculation models are shown in Fig. 18 and Fig. 2(b).

Table 3: Parameters of the foundation soil

Homogeneous foundation	Shear wave velocity (m/s)	Poisson's ratio	Density (kg/m^3)
soil 1	124	0.31	1847
soil 2	200	0.31	1847
soil 3	260	0.31	1847

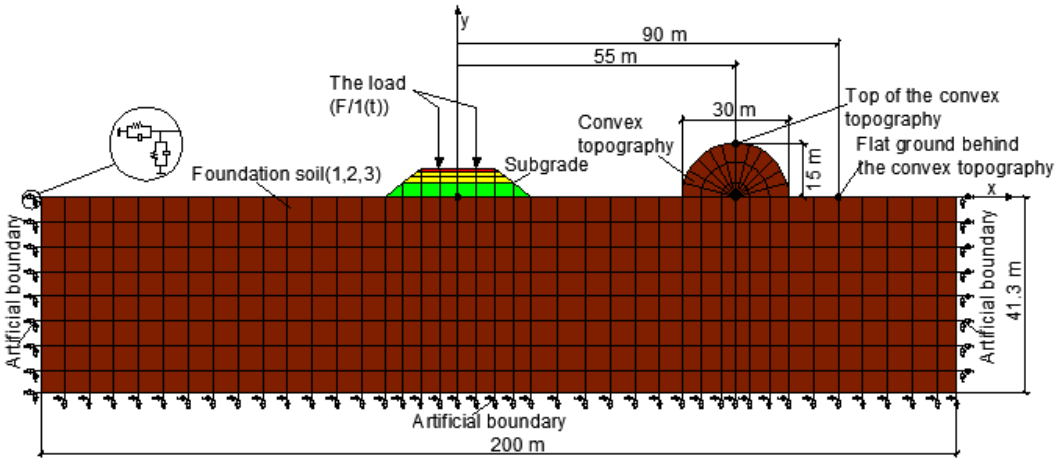

Figure 18: Calculation model of a subgrade-convex topography with different foundation soil

Fig. 19 and Fig. 20 show that the ground vibrations on the convex topography (40 m to 70 m from the track centerline) and flat ground behind it are both stronger when the foundation soil is softer. However, the effects of the foundation soil properties at different locations are still somewhat different. Thus, Fig. 21 and Fig. 22 are added to give a clearer indication of the responses at different locations.

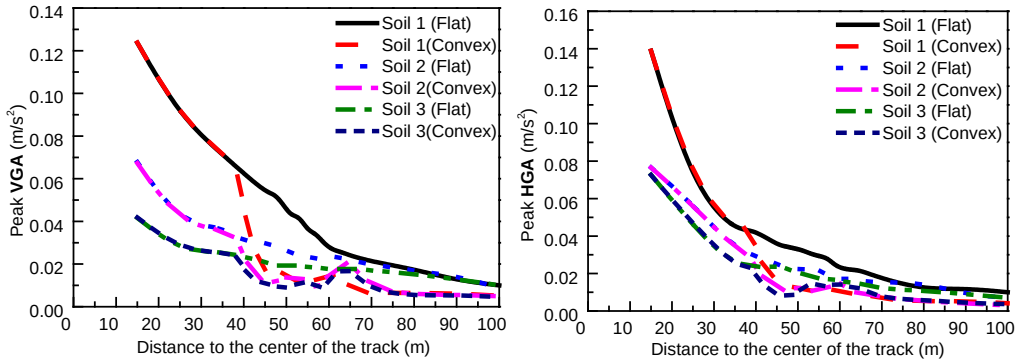

(a) (b)

Figure 19: Peak acceleration of three kinds of foundation soil

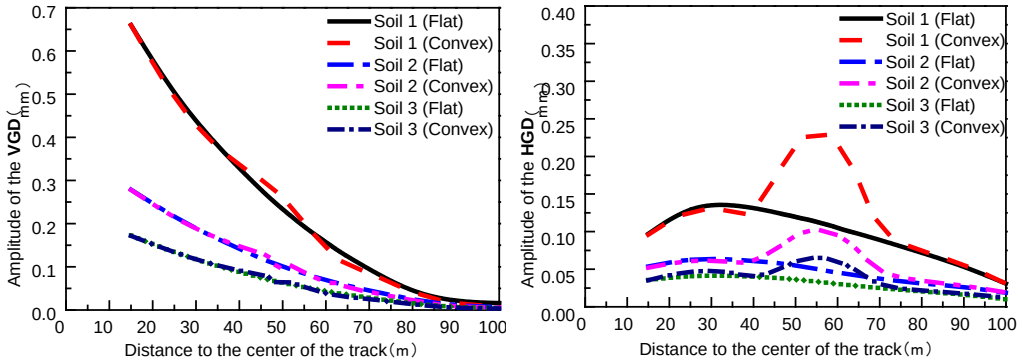

Figure 20: Amplitude of ground displacements of three kinds of foundation soil

As shown in Fig. 21, comparing with the response of the flat topography (without a convex topography), the decreased amplitudes of the VGA and HGA reduce significantly at the top of the convex topography as the foundation soil hardens (from soil 1 to soil 3). Another point to note is that the change of the foundation soil has little impact on amplification effect of the VGD and HGD at the top of the convex topography (55 m from the track centerline).

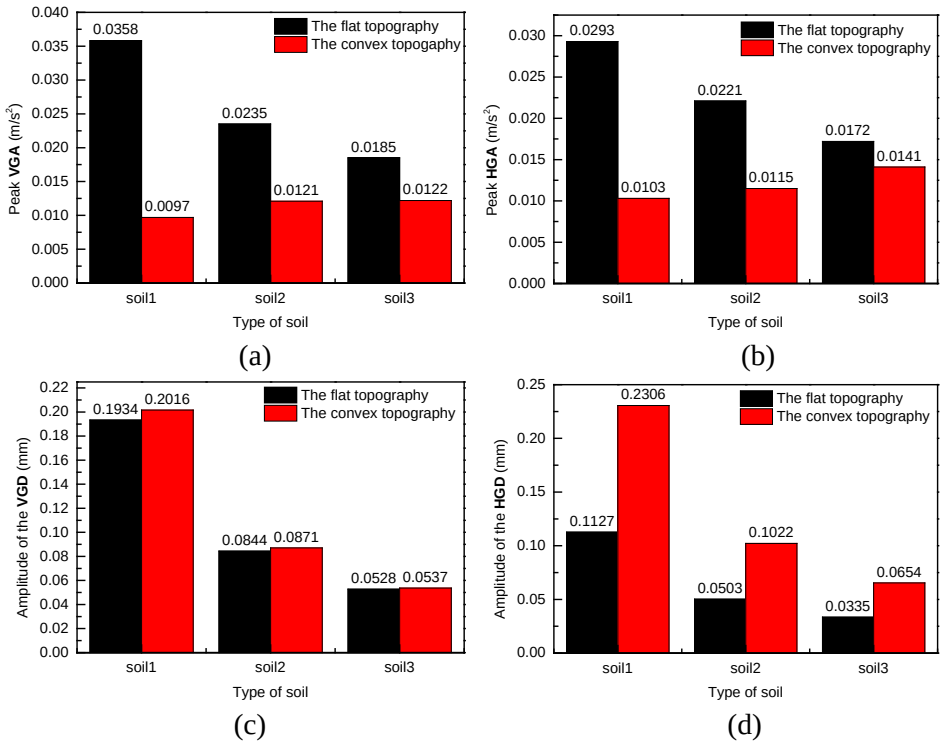

Figure 21: The Comparison of the accelerations and displacements regarding the flat topography and convex topography at 55 m from the track centerline for three kinds of foundation soil

Fig. 22 displays that the hardened foundation soil reduces the decreased amplitudes of the VGA, HGA and VGD on the flat ground behind the convex topography, but the impacts are not obvious. Moreover, the influence of the hardened foundation soil on the amplification effect of the HGD on the flat ground behind the convex topography can be ignored. The amplification multiples of the HGDs of three foundation soil are all approximately 1.06 times.

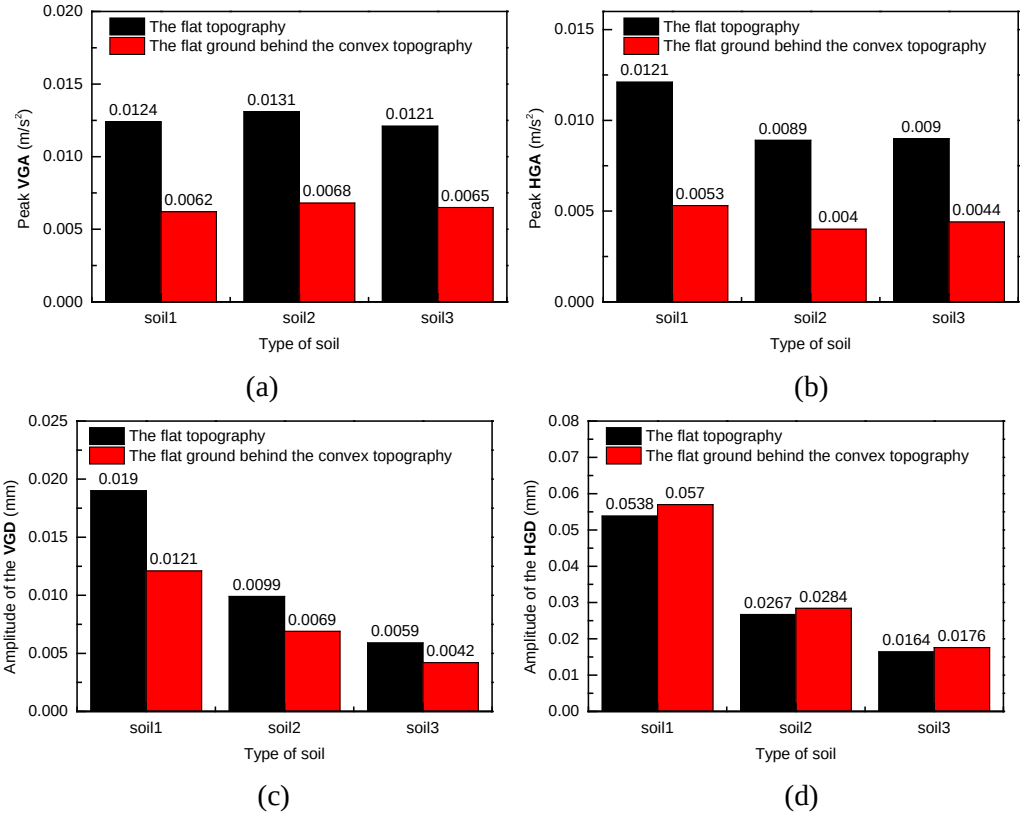

Figure 22: The Comparison of the accelerations and displacements regarding the flat topography and flat ground at 90 m from the track centerline for three kinds of foundation soil

From the above results it can be seen that the convex topographic effect is weakened when the foundation soil becomes hard, and it is more obvious on the convex topography than on the flat ground behind it.

Fig. 23 shows that at the top of the convex topography or on the flat ground behind it, the high-frequency components (20-25 Hz) are more obviously attenuated by the convex topography as the foundation becomes softer. In other words, the high-frequency components (20-25 Hz) of the vibrations are more abundant when the foundation is harder.

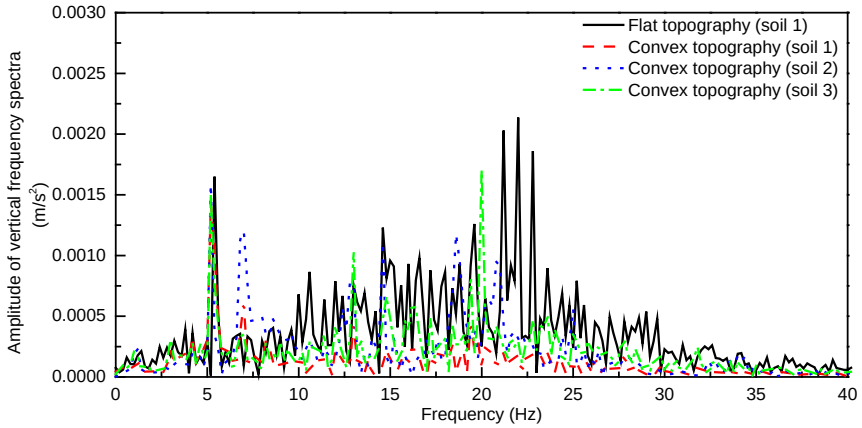
Flat topography (soil 1)
Convex topography (soil 1)
Convex topography (soil 2)
Convex topography (soil 3)
Amplitude of vertical frequency spectra (m/s²)
Frequency (Hz)
0.0030
0.0025
0.0020
0.0015
0.0010
0.0005
0.0000
0
5
10
15
20
25
30
35
40

(a)

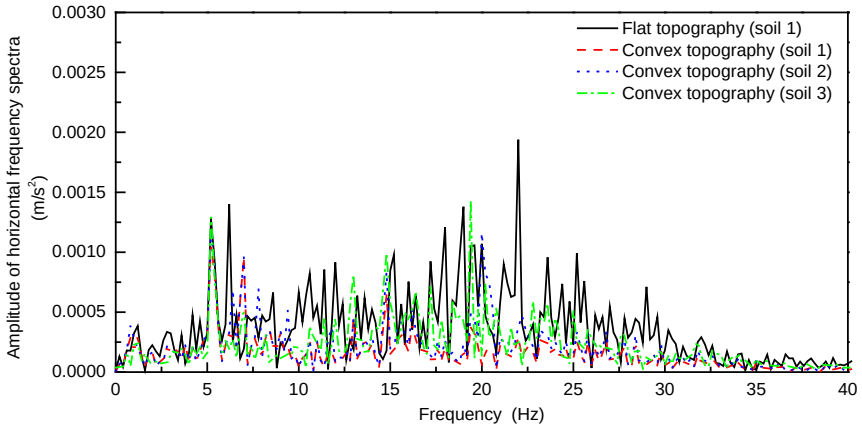
Flat topography (soil 1)
Convex topography (soil 1)
Convex topography (soil 2)
Convex topography (soil 3)
Amplitude of horizontal frequency spectra (m/s²)
Frequency (Hz)
0.0030
0.0025
0.0020
0.0015
0.0010
0.0005
0.0000
0
5
10
15
20
25
30
35
40

(b)

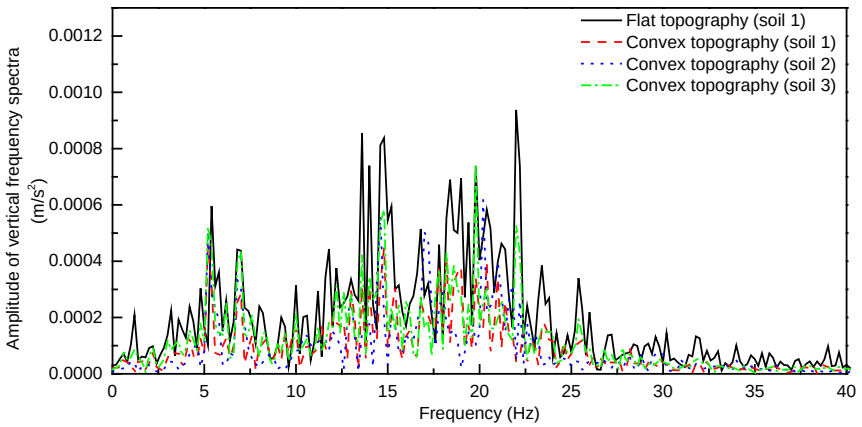
Flat topography (soil 1)
Convex topography (soil 1)
Convex topography (soil 2)
Convex topography (soil 3)
Amplitude of vertical frequency spectra (m/s²)
Frequency (Hz)
0.0012
0.0010
0.0008
0.0006
0.0004
0.0002
0.0000
0
5
10
15
20
25
30
35
40

(c)

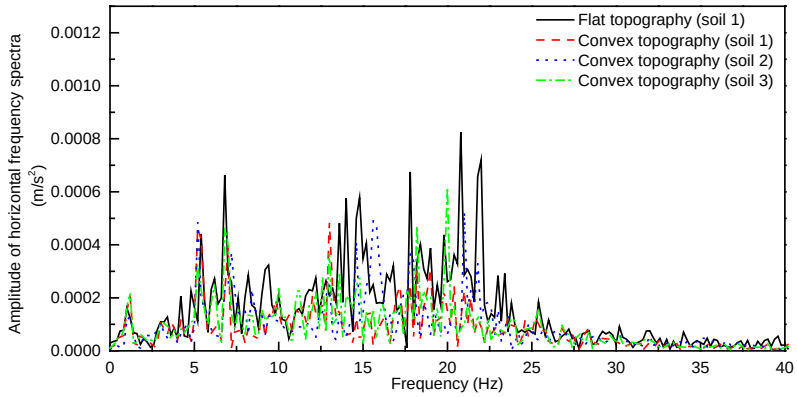

(d)

Figure 23: Frequency spectra of three kinds of foundation soil. (a) Vertical frequency spectra of the top of the convex topography. (b) Horizontal frequency spectra of the top of the convex topography. (c) Vertical frequency spectra of the flat ground behind the convex topography. (d) Horizontal frequency spectra of the flat ground behind the convex topography

5 Conclusions

In this paper, the 2D finite element models of the subgrade-convex topography and subgrade-flat topography subjected to train load were established, and the influence regularities of the bottom width, cross-sectional shape and height-width ratio of the convex topography and the foundation soil properties on the train-induced vibration are analyzed. The following conclusions are obtained:

1) The VGA and HGA on the convex topography are decreased, but the VGD and HGD are amplified. The amplification effect of the VGD and HGD is more obvious as the bottom width of the convex topography increases. The HGD is amplified by energy concentration at the top of the triangular convex topography. In addition, the VGA and HGD on the convex topography decrease more obviously with the increase of the height-width ratio. Another point to note is that the convex topographic effects are weakened as the foundation soil hardens.

2) The VGA, HGA and VGD on the flat ground behind the convex topography are obviously decreased, but the HGD is amplified. The amplification effect of the HGD is more obvious as the bottom width of the convex topography increases. Moreover, the cross-sectional shape and height-width ratio of the convex topography and the hardness of the foundation soil have little effect on the vibration responses caused by trains on the flat ground behind the convex topography.

3) The vertical and horizontal high-frequency components (20-25 Hz) at the top of the convex topography and on the flat ground behind it will be obviously attenuated. The vertical and horizontal high-frequency components are more obviously attenuated as the height-width ratio of the convex topography increases. Furthermore, the high-frequency components are more abundant as the foundation soil hardens.

Acknowledgement: This work is supported by the National Natural Science Foundation of China (Grant No. 51868022) and the National Science Foundation for Young Scientists of China (Grant No. 51808219).

References

Auersch, L. (2008): *The Influence of the Soil on Track Dynamics and Ground-Borne Vibration*. Springer Berlin Heidelberg, Germany.

Auersch, L. (2012): Train induced ground vibrations: different amplitude-speed relations for two layered soils. *Proceedings of the Institution of Mechanical Engineers Part F-Journal of Rail and Rapid Transit*, vol. 226, no. 5, pp. 469-488.

Auersch, L.; Reitan, A. (1994): Wave propagation in layered soil: theoretical solution in wavenumber domain and experimental results of hammer and railway traffic excitation. *Journal of Sound and Vibration*, vol. 173, no. 2, pp. 233-264.

Chen, R.; Zhao, X.; Wang, Z.; Jiang, H. G.; Bian, X. C. (2013): Experimental study on dynamic load magnification factor for ballastless track-subgrade of high-speed railway. *Journal of Rock Mechanics and Geotechnical Engineering*, vol. 5, no. 4, pp. 306-311.

Connolly, D.; Giannopoulos, A.; Forde, M. C. (2013): Numerical modelling of ground borne vibrations from high speed rail lines on embankments. *Soil Dynamics and Earthquake Engineering*, vol. 46, no. 1, pp. 13-19.

Connolly, D. P.; Costa, P. A.; Kouroussis, G.; Galvin, P.; Woodward, P. K. et al. (2015): Large scale international testing of railway ground vibrations across Europe. *Soil Dynamics and Earthquake Engineering*, vol. 71, pp. 1-12.

Degrande, G.; Schillemans, L. (2001): Free field vibrations during the passage of a Thalys high-speed train at variable speed. *Journal of Sound and Vibration*, vol. 247, no. 1, pp. 131-144.

Feng, S. J.; Zhang, X. L.; Zheng, Q. T.; Wang, L. (2017): Simulation and mitigation analysis of ground vibrations induced by high-speed train with three dimensional FEM. *Soil Dynamics and Earthquake Engineering*, vol. 94, pp. 204-214.

Ghayamghamian, M. R.; Kawakami, H. (2000): On-site nonlinear hysteresis curves and dynamic soil properties. *Journal of Geotechnical and Geoenvironmental Engineering*, vol. 126, no. 6, pp. 543-555.

Hall, L. (2003): Simulations and analyses of train-induced ground vibrations in finite element models. *Soil Dynamics and Earthquake Engineering*, vol. 23, no. 5, pp. 403-413.

Hesami, S.; Ahmadi, S.; Ghalesari, A. T. (2016): Numerical modeling of train-induced vibration of nearby multi-story building: A case study. *KSCE Journal of Civil Engineering*, vol. 20, no. 5. pp. 1701-1713.

Jenkins, H. H.; Stephenson, J. E.; Clayton, G. A.; Morland, G. W.; Lyton, D. (1974): The effect of track and vehicle parameters on wheel/rail vertical dynamic loads. *Railway Engineering Journal*, vol. 3, no. 1, pp. 2-16.

Jones, D. V.; Houedec, D. L.; Peplow, A. T. (1998a): Ground vibration in the vicinity of a moving harmonic rectangular load on a half-space. *European Journal of Mechanics-A/Solids*, vol. 17, no. 1, pp. 153-166.

Jones, D. V.; Houedec, D. L.; Petyt, M. (1998b): Ground vibration due to a rectangular harmonic load. *Journal of Sound and Vibration*, vol. 212, no. 1, pp. 61-74.

Kausel, E.; Roesset, J. M.; Christian, J. T. (1976): Nonlinear behavior in soil-structure interaction. *Journal of the Geotechnical Engineering Division*, vol. 102, pp. 1159-1170.

Kim, D. S.; Lee, J. S. (2000): Propagation and attenuation characteristics of various ground vibrations. *Soil Dynamics and Earthquake Engineering*, vol. 19, no. 2, pp. 115-126.

Kouroussis, G.; Conti, C.; Verlinden, O. (2013): Investigating the influence of soil properties on railway traffic vibration using a numerical model. *Vehicle System Dynamics*, vol. 51, no. 3, pp. 421-442.

Krylov, V. V. (1997): Spectra of low-frequency ground vibrations generated by high-speed trains on layered ground. *Journal of Low Frequency Noise Vibration and Active Control*, vol. 16, no. 4, pp. 257-270.

Kuhlemeyer, R. L.; Lysmer, J. (1973): Finite element method accuracy for wave propagation problems. *Journal of Soil Mechanics and Foundations Division*, vol. 99, no. 5, pp. 421-427.

Liu, J. B. (1996): The effect of local irregular topography on seismic ground motion. *Acta Seismologica Sinica*, vol. 9, no. 2. pp. 309-315.

Liu, J.; Lu, Y. (1998): A direct method for analysis of dynamic soil-structure interaction based on interface idea. *Developments in Geotechnical Engineering*, vol. 83, no. 3, pp. 261-276.

Lopes, P.; Costa, P. A.; Ferraz, M.; Calcada, R.; Cardoso, S. A. (2014): Numerical modeling of vibrations induced by railway traffic in tunnels: From the source to the nearby buildings. *Soil Dynamics and Earthquake Engineering*, vol. 61-62, no. 3, pp. 269-285.

Shao, M. H.; Wei, K.; Han, H. Y. (2013): Investigation into ground-born vibration characteristic induced by high-speed non-ballasted railway. *Journal of Chongqing University of Technology (Natural Science)*, vol. 27, no. 9, pp. 53-58 (In Chinese).

Sheng, X.; Jones, C. J. C.; Petyt, M. (1999): Ground vibration generated by a harmonic load acting on a railway track. *Journal of Sound and Vibration*, vol. 225, no. 1, pp. 3-28.

Sohrabi-Bidar, A.; Kamalian, M. (2013): Effects of three-dimensionality on seismic response of Gaussian-shaped hills for simple incident pulses. *Soil Dynamics and Earthquake Engineering*, vol. 52, no. 13, pp. 1-12.

Sohrabi-Bidar, A.; Kamalian, M.; Jafari, M. K. (2010): Seismic response of 3-D Gaussian-shaped valleys to vertically propagating incident waves. *Geophysical Journal International*, vol. 183, no. 3, pp. 1429-1442.

Takemiya, H. (2008): Analyses of wave field from high-speed train on viaduct at shallow/deep soft grounds. *Journal of Sound and Vibration*, vol. 310, no. 3, pp. 631-649.

Taniguchi, E.; Sawada, K. (1979): Attenuation with distance of traffic-induced vibrations. *Journal of the Japanese Society of Soil Mechanics and Foundation Engineering*, vol. 19, no. 2, pp. 15-28.

Xia, H.; Cao, Y. M.; Roeck, G. D. (2010): Theoretical modeling and characteristic analysis of moving-train induced ground vibrations. *Journal of Sound and Vibration*, vol. 329, no. 7, pp. 819- 832.

Zhai, W. M. (2007): *Vehicle-Track Coupling Dynamics*. Science Press, China (In Chinese).

Zhang, L.; Feng, Q. (2011): Experimental analysis on ground vibration generated by high-speed train. *International Conference on Transportation Engineering*, vol. 23, no. 1, pp. 1597-1602.